Journal of Controlled Release xxx (2014) xxx–xxx

Contents lists available at ScienceDirect

Journal of Controlled Release

journal homepage: www.elsevier.com/locate/jconrel

Avidity-controlled hydrogels for injectable co-delivery of induced pluripotent stem cell-derived endothelial cells and growth factors

Widya Mulyasasmita [a], Lei Cai [b,c], Ruby E. Dewi [b], Arshi Jha [c,d], Sabrina D. Ullmann [e], Richard H. Luong [f], Ngan F. Huang [c,d,g], Sarah C. Heilshorn [a,b,c,*]

[a] Department of Bioengineering, Stanford University, Stanford, CA, USA
[b] Department of Materials Science and Engineering, Stanford University, Stanford, CA, USA
[c] Stanford Cardiovascular Institute, Stanford University, Stanford, CA, USA
[d] Veterans Affairs Palo Alto Health Care System, Palo Alto, CA, USA
[e] Department of Chemistry, RWTH Aachen University, Aachen, Germany
[f] Department of Comparative Medicine, Stanford University, Stanford, CA, USA
[g] Division of Cardiovascular Medicine, Stanford University, Stanford, CA, USA

ARTICLE INFO

Article history:
Received 11 April 2014
Accepted 8 May 2014
Available online xxxx

Keywords:
iPSC
Hydrogel
Protein engineering
VEGF
Endothelial cell

ABSTRACT

To translate recent advances in induced pluripotent stem cell biology to clinical regenerative medicine therapies, new strategies to control the co-delivery of cells and growth factors are needed. Building on our previous work designing Mixing-Induced Two-Component Hydrogels (MITCHs) from engineered proteins, here we develop protein–polyethylene glycol (PEG) hybrid hydrogels, MITCH-PEG, which form physical gels upon mixing for cell and growth factor co-delivery. MITCH-PEG is a mixture of C7, which is a linear, engineered protein containing seven repeats of the CC43 WW peptide domain (C), and 8-arm star-shaped PEG conjugated with either one or two repeats of a proline-rich peptide to each arm (P1 or P2, respectively). Both 20 kDa and 40 kDa star-shaped PEG variants were investigated, and all four PEG-peptide variants were able to undergo a sol–gel phase transition when mixed with the linear C7 protein at constant physiological conditions due to noncovalent heterodimerization between the C and P domains. Due to the dynamic nature of the C–P physical crosslinks, all four gels were observed to be reversibly shear-thinning and self-healing. The P2 variants exhibited higher storage moduli than the P1 variants, demonstrating the ability to tune the hydrogel bulk properties through a biomimetic peptide-avidity strategy. The 20 kDa PEG variants exhibited slower release of encapsulated vascular endothelial growth factor (VEGF), due to a decrease in hydrogel mesh size relative to the 40 kDa variants. Human induced pluripotent stem cell-derived endothelial cells (hiPSC-ECs) adopted a well-spread morphology within three-dimensional MITCH-PEG cultures, and MITCH-PEG provided significant protection from cell damage during ejection through a fine-gauge syringe needle. In a mouse hindlimb ischemia model of peripheral arterial disease, MITCH-PEG co-delivery of hiPSC-ECs and VEGF was found to reduce inflammation and promote muscle tissue regeneration compared to a saline control.

1. Introduction

We introduce a new family of injectable hydrogels formed through the dynamic hetero-assembly of a linear, engineered protein with a star-shaped, peptide-modified PEG molecule that takes advantage of biomimetic avidity to fine-tune the hydrogel properties. Following the first report of Mixing-Induced Two-Component Hydrogels (MITCHs), which were composed entirely of linear, engineered proteins [1], the strategy was expanded by several groups to demonstrate the successful mixing-induced gelation of star-shaped, peptide-modified PEG molecules using a variety of peptide binding domains [2–6]. In all of these systems, gelation is induced by noncovalent peptide hetero-assembly when the individual hydrogel components are mixed together. Because the mechanical properties of MITCH systems are directly related to the concentration and binding affinity of the hetero-assembled crosslinks [1,7], we hypothesized that presenting dimers of binding ligands in close proximity would result in a dramatic lowering of the apparent equilibrium dissociation constant, $K_{d,app}$, and hence increase the number of hetero-assembled crosslinks. This gelation mechanism mimics the evolved strategy of avidity, *i.e.* the combined enhancement of multiple weak affinity interactions. At a molecular level, avidity can be mechanistically explained by considering the dynamic, noncovalent binding of a single protein receptor to a single ligand within a larger array of ligands. Although the protein receptor will bind and unbind

* Corresponding author at: 476 Lomita Mall, McCullough Room 246, Stanford University, Stanford, CA 94305-4045, USA. Tel.: +1 650 723 3763; fax: +1 650 498 5596.
E-mail address: heilshorn@stanford.edu (S.C. Heilshorn).

http://dx.doi.org/10.1016/j.jconrel.2014.05.015
0168-3659/

the ligand with the kinetic rate constants, k_{on} and k_{off}, the likelihood of the unbound receptor quickly finding another ligand to rebind will increase as the ligand density increases. Therefore, the apparent k_{on} also increases with ligand density, effectively lowering the apparent equilibrium dissociation constant. As a result, multiple weak binding interactions can appear to have a much higher effective binding energy. While this avidity-based, multivalent strategy has been widely applied in the field of nanobiotechnology for drug delivery, bioimaging, and biosensing applications [8–10], it has yet to be explored in peptide hetero-assembled hydrogels.

We further hypothesized that these avidity-controlled MITCH systems would be tunable carriers for the co-delivery of induced pluripotent stem cell-derived endothelial cells and growth factors. Human-induced pluripotent stem cell-derived endothelial cells (hiPSC-ECs) are ideal candidates for vascular therapy. Reprogrammed from somatic cells, iPSCs offer an abundant source of autologous cells that mitigate immunogenicity and ethical concerns [11]. In a murine hindlimb ischemia model for peripheral arterial disease (PAD), hiPSC-ECs injected into the ischemic calf muscle enhanced microvessel density and improved blood reperfusion by secreting angiogenic cytokines and incorporating into expanding endogenous microvasculature [12]. The clinical adoption of hiPSC-EC therapy is currently hampered by the rapid decline of transplanted cell viability, which necessitates multiple cell administrations for sustaining therapeutic efficacy [12]. Acutely, the number of viable cells plummets during injection due to membrane-disruptive extensional forces experienced in the syringe needle [13]. Pre-encapsulation of cells within a shear-thinning, self-healing physical hydrogel can provide significant protection from these mechanical forces [13–15]; therefore, we hypothesized that avidity-controlled MITCH systems may provide a similar protective effect.

Without the aid of a biomaterial carrier, efforts to enhance transplanted cell survival typically involve donor cell supplementation with biochemical factors that block apoptotic pathways associated with hypoxia and inflammatory insult [16,17]. Vascular endothelial growth factor (VEGF) is a promising drug for co-delivery with hiPSC-ECs into ischemic target tissues, since VEGF is known to promote endothelial cell proliferation, survival and migration. In addition to enhancing donor cell survival, VEGF is a potent pro-angiogenic signal that could augment hiPSC-EC paracrine signaling and improve blood reperfusion by coaxing endogenous revascularization. Similar to many soluble pro-survival factors [18], VEGF has a short *in vivo* circulating half-life (3 min in mice) [19]. Moreover, bolus delivery of VEGF results in a rapid dosage burst that produces leaky and aberrant vessels and off-target effects [20] instead of mature and stable vasculature. In a murine hindlimb ischemia model, optimal revascularization was achieved by a profile of high initial VEGF dosage, followed by steadily decreasing concentration over time [20]. Temporal regulation therefore underpins the safety and efficacy of cell and VEGF combinatorial therapy.

Previously, several types of hydrogel scaffolds have been used to deliver cells and angiogenic growth factors separately or in combination to increase vascularization in ischemic models [21–23]. These hydrogels include collagen–fibronectin [24], alginate [24,25], fibrin [26], gelatin [27], poly(lactide-co-glycolide) (PLGA) [28,29], and peptide amphiphiles [30]. A collagen–fibronectin gel that encapsulated VEGF-loaded alginate microparticles and endothelial cells was implanted into the gastrocnemius muscle of mice with induced hindlimb ischemia [24]. VEGF released from the microparticles increased the survival of the transplanted endothelial cells and enhanced muscle myoglobin expression, a sign of recovery from ischemia, compared to solely cell transplantation or VEGF delivery [24]. This synergistic angiogenic effect was also demonstrated by implanting fibrin scaffolds containing angiogenic growth factors and directly injecting bone marrow cells to the murine ischemic muscles [26]. While these implanted hydrogel scaffolds showed enhanced neovascularization by co-delivery of cells and growth factors, the gels were not injectable and required surgical implantation. Furthermore, these scaffolds, which are based on harvested biopolymers (*e.g.* collagen, fibronectin, fibrin), offer limited control over the material properties compared to engineered matrices.

To demonstrate the suitability of our newly developed avidity-controlled MITCH system for injectable co-delivery of hiPSC-ECs and VEGF, we synthesized and characterized a family of four hydrogels with tunable viscoelastic and diffusive properties. As proof of concept, we further evaluated the lead formulation in a preclinical murine hindlimb ischemia model of peripheral arterial disease. To the best of our knowledge, this work represents the first demonstration of avidity-controlled, injectable hydrogels for applications in regenerative cell and drug combination therapy.

2. Materials and methods

2.1. Synthesis and purification of C7 protein

The C7 recombinant protein polymer (see Fig. S1 for full amino acid sequence) was cloned, synthesized, and purified as reported previously [1]. In brief, the DNA sequence encoding the C7 block copolymer was cloned into the pET-15b vector (Novagen) and transformed into the BL21(DE3)pLysS *Escherichia coli* host strain (Life Technologies). Protein was expressed following isopropyl β-D-1-thiogalactopyranoside (IPTG) induction, purified by affinity chromatography *via* the specific binding of N-terminal polyhistidine tag to Ni-nitrilotriacetic acid resin (Qiagen), buffer exchanged into phosphate-buffered saline (PBS), and concentrated by diafiltration across Amicon Ultracel filter units (Millipore) with 30 kDa Molecular Weight Cut-Off (MWCO). Protein identity and purity were confirmed by gel electrophoresis, MALDI-TOF mass spectrometry, and amino acid compositional analysis (data not shown).

C7 protein used in *in vivo* experiments was further subjected to lipopolysaccharide (LPS) removal by four cycles of phase separation and temperature transition extraction with Triton X-114. Residual Triton X-114 was removed by overnight incubation with Bio-Beads SM-2 Adsorbents (Biorad), and the PyroGene Recombinant Factor C Endotoxin Detection Assay kit (Lonza) was used to confirm the reduction of LPS levels to below 5 EU/mg in the final C7 protein solutions.

2.2. Conjugation of P1 and P2 peptides to 8-arm PEG

8-Arm polyethylene glycol vinyl sulfone (8-arm-PEG-VS) with nominal molecular weights of 20 and 40 kDa were purchased from Nanocs (Boston, MA). Peptides P1 (EYPPYPPPPYPSGC, 1563 Da) and P2 (EYPPYPPPPYPSGGGGGEYPPYPPPPYPSGC, 3234 Da) were purchased through custom peptide synthesis from Genscript Corp (Piscataway, NJ, USA) and confirmed to have purity of 92–98% by HPLC. All other chemicals were purchased from Sigma-Aldrich (Milwaukee, WI) unless otherwise noted. A Michael-type addition of P1 or P2 to 8-arm-PEG-VSs was conducted in a Schlenk tube in the presence of tris(2-carboxyethyl)phosphine (TCEP). Peptides (P1 or P2), 8-arm-PEG-VS (20 kDa or 40 kDa), and TCEP were dissolved at a molar ratio of thio:VS:TCEP = 1.5:1:0.05 in 0.3 M triethanolamine (TEA) solution and pH was adjusted to 8.0. The reaction solution was then degassed, flushed with nitrogen, and maintained in a 37 °C incubator for 24 h. The solution was then lyophilized and washed with chloroform to remove unreacted PEG. The precipitate was redissolved and dialyzed into deionized water, using 10 kDa MWCO dialysis tubing. A second lyophilization step yielded the final 8-arm-PEG–peptide conjugate products as white powder, with overall conjugation efficiency of ~80%.

The chemical structures of the purified 8-arm-PEG–peptide conjugates were confirmed by ^{1}H Nuclear Magnetic Resonance (NMR) spectrometry, acquired on a Varian Inova 500 MHz NMR spectrometer. Deuterium oxide containing a trace amount of 4,4-dimethyl-4-silapentane-1-sulfonic acid (DSS) (Cambridge Isotope Laboratories, Andover, MA) was used as a solvent. Peptide conjugation efficiency was quantified from the ratio of the area under the tyrosine doublets to the peak area corresponding to the PEG backbone. Compositional purity was characterized by polyacrylamide gel electrophoresis (PAGE) under non-denaturing conditions. Bands were visualized by staining with Coomassie brilliant blue dye.

2.3. Isothermal titration calorimetry (ITC)

The differential binding affinity of P1 and P2 peptides to C1 (a single CC43 WW domain) was studied by measuring enthalpy changes using a Nano ITC instrument (TA Instruments, New Castle, DE, USA). All peptides were dissolved and dialyzed overnight (MWCO = 1.0 kDa) against PBS (pH 7.4) to ensure buffer matching. 2 mM of C1 solution was loaded in the injection syringe and titrated into 0.2 mM P1 or P2 solution in the sample cell in a sequence of 16 injections of 3 μL volumes. Successive injections were delayed by 5 min to allow equilibration. All experiments were conducted at 25 °C with constant stirring at 300 rpm. The NanoAnalyze software was used to transform raw heat against injection number into enthalpy change per mole of injectant against molar ratio. The integrated isotherms were then fitted to an independent site model to obtain thermodynamic parameters of binding.

Please cite this article as: W. Mulyasasmita, et al., Avidity-controlled hydrogels for injectable co-delivery of induced pluripotent stem cell-derived endothelial cells and growth fact..., J. Control. Release (2014), http://dx.doi.org/10.1016/j.jconrel.2014.05.015

2.4. Bulk rheological measurement

Each WW domain in C7 is treated as one C unit. Since ITC measurements revealed that both P1 and P2 bind to C1 with approximately 1:1 stoichiometry, each pendant peptide group (P1 or P2) in the 8-arm-PEG–peptide conjugates was treated as one P unit regardless of multivalency. Thus, in calculating C:P ratios, P2 is considered as one P unit even though it has two repeats of the proline-rich peptide domain.

Unless otherwise specified, MITCH variants 8P1-20k, 8P2-20k, 8P1-40k, and 8P2-40k refer to hydrogel mixtures of C7 and 8-arm-PEG–P1 (20 kDa), 8-arm-PEG–P2 (20 kDa), 8-arm-PEG–P1 (40 kDa), and 8-arm-PEG–P2 (40 kDa), respectively, mixed to achieve a final concentration of 10% w/v and a C:P ratio of 1:1.

Dynamic oscillatory rheology experiments were performed on a stress-controlled rheometer (AR-G2, TA instrument, New Castle, DE) using a 25-mm diameter cone–plate geometry. Gel samples were prepared by mixing equal volumes of 10% w/v 8-arm-PEG–peptide conjugates with 10% w/v C7, at volume ratios corresponding to various C:P stoichiometric ratios. Samples were loaded immediately onto the rheometer, and a humidity chamber was secured in place to prevent dehydration. Frequency sweeps at 37 °C were performed at 5% constant strain to obtain storage modulus G' and loss modulus G''.

Shear-thinning and self healing properties of the gel samples (8P1-20k, 8P2-20k, 8P1-40k, and 8P2-40k, concentration = 10% w/v, C:P ratio = 1:1) were characterized at 37 °C by measuring linear viscosities (η) under a time sweep mode, at alternating low and high shear rates of 0.1 s^{-1} and 10 s^{-1}, respectively, for 30 s each and a total of 150 s.

2.5. Fluorescence recovery after photobleaching (FRAP) diffusivity measurement

Fluorescence recovery after photobleaching (FRAP) measurement was performed using dextran (MW = 20, 40, and 70 kDa) conjugated to fluorescein isothiocyanate (FITC) (Invitrogen). Dextran was individually mixed with various MITCH-PEG formulations (8P1-20k, 8P2-20k, 8P1-40k, and 8P2-40k; gel volume = 30 μL, concentration = 10% w/v, C:P ratio = 1:1) at a final dextran concentration of 4 mg/mL, and the total fluorescence intensity was visualized at 37 °C using a Leica TCS SP5 confocal microscope at low light intensity. Photobleaching was done by exposing a 100 × 100 μm spot in the field of view to high intensity laser light. A series of images were taken every 3 s for 5 min to track the recovery of fluorescence. Control experiments were also performed using PBS, rat-tail Type I collagen (2 mg/mL, BD Biosciences), and growth-factor-reduced Matrigel (BD Biosciences) as diffusion media, prepared according to manufacturers' protocols. The resulting fluorescence recovery profiles were modeled by Fickian diffusion according to a previously reported method to calculate dextran diffusivities [31].

2.6. Kinetics of hydrogel erosion and dextran and VEGF release

MITCH-PEG formulations (8P1-20k, 8P2-20k, 8P1-40k, and 8P2-40k; gel volume = 30 μL, concentration = 10% w/v, C:P ratio = 1:1) were formed by mixing the PEG–peptide component and C7 in a circular silicone mold (diameter = 4 mm, height = 2 mm) within a 24-well plate (n ≥ 3). The mixture was allowed to undergo sol–gel phase transition for 15 min at 37 °C in a humidified incubator, after which 1.5 mL of PBS was added to each well. Sampling volumes of 100 μL were obtained from the PBS supernatant and wells were replenished with 100 μL of fresh PBS over a period of 14 days. Gel erosion kinetics were studied by using absorbance spectroscopy at 280 nm (SpectraMax M2 Spectrophotometer, Molecular Devices) to measure the amount of protein released into the supernatant at each time point.

To study dextran release kinetics, 20 kDa FITC–dextran (Invitrogen) was encapsulated in various MITCH-PEG formulations (8P1-20k, 8P2-20k, 8P1-40k, and 8P2-40k; gel volume = 30 μL, concentration = 10% w/v, C:P ratio = 1:1) by first mixing with the PEG–peptide component and subsequently with C7 in a circular silicone mold (diameter = 4 mm, height = 2 mm) within a 24-well plate (n ≥ 3). The initial amount of dextran in each gel was 6 μg, at a concentration of 0.2 mg/mL. The mixture was allowed to gel for 15 min at 37 °C in a humidified incubator, after which 1.5 mL of PBS was added to each well. Release kinetics were followed by sampling and replenishing 100 μL of the PBS supernatant over a period of 14 days. The amount of dextran that had been released in the sampling volume was quantified using a SpectraMax M2 Spectrophotometer (Molecular Devices) to measure fluorescence at 488 nm.

Recombinant human $VEGF_{165}$ (carrier free, R&D Systems) was dissolved in PBS (supplemented with 0.1% w/v BSA) and encapsulated in various MITCH-PEG formulations (8P1-20k, 8P2-20k, 8P1-40k, and 8P2-40k; gel volume = 30 μL, concentration = 10% w/v, C:P ratio = 1:1) by first mixing with the PEG–peptide component and subsequently with C7 in a circular silicone mold (diameter = 4 mm, height = 2 mm) within a 24-well plate (n ≥ 3). The initial amount of VEGF in each gel was 3 μg, at a concentration of 0.1 mg/mL. The mixture was allowed to gel for 15 min at 37 °C in a humidified incubator, after which 1.5 mL of PBS (supplemented with 0.1% w/v BSA) was added to each well. Release kinetics were followed by sampling and replenishing 100 μL of the PBS supernatant over a period of 14 days. Samples were frozen at −80 °C immediately after collection and thawed prior to quantification. The amount of VEGF present in the supernatant at each time point was quantified using Human VEGF Quantikine ELISA Kit (R&D Systems), according to the manufacturer's protocol.

2.7. Cell culture and maintenance

Human induced pluripotent stem cells (hiPSCs) were generated from adult dermal fibroblasts using retroviral constructs encoding Oct4, Sox2, c-Myc and Klf4, as described previously [12]. hiPSCs were cultured on mouse embryonic fibroblast feeder cells and maintained in standard WiCell human embryonic growth medium supplemented with 10 ng/mL basic fibroblast growth factor. Endothelial differentiation was initiated by incubating confluent cultures of hiPSCs with 1 mg/mL type IV collagenase for 10 min. Cells were then transferred to ultra low attachment dishes and cultured in differentiation medium (α-Minimum Eagle's Medium, 20% fetal bovine serum, L-glutamine, β-mercaptoethanol (0.05 mmol/L), 1% non-essential amino acids, bone morphogenetic protein-4 (BMP-4, 50 ng/mL, Peprotech), and vascular endothelial growth factor (VEGF-A, 50 ng/mL, Peprotech)) for 4 days to form embryoid bodies (EBs). On day 4, EBs were reattached to gelatin-coated dishes and further supplemented with VEGF-A for 10 days before purification. Differentiation medium was changed every 2 days.

On day 14 of differentiation, hiPSC-derived endothelial cells (hiPSC-ECs) were dissociated into single cells and purified by fluorescence activated cell sorting (FACS) using CD31 antibody (eBiosciences). Endothelial identity of the purified hiPSC-ECs was characterized following protocols reported in previous publications [12,32]. To facilitate non-invasive tracking, hiPSC-ECs were lentivirally transduced with a double fusion reporter construct encoding firefly luciferase (Fluc) and enhanced green fluorescence protein (eGFP) under a ubiquitin promoter [12]. For use in cell encapsulation and injection experiments, hiPSC-ECs (Fluc+/eGFP+) were expanded in EGM-2MV medium (Lonza).

2.8. In vitro cell encapsulation, injection, and quantification of viability

All *in vitro* encapsulation and injection experiments were performed with 25 μL gel volumes containing 3.3×10^4 cells. hiPSC-ECs were trypsinized and resuspended to a density of 6.7×10^6 cells/mL in EGM-2MV media. Cell suspension (5 μL) was first mixed with the 8-arm PEG–peptide conjugate solution (20% w/v in PBS) and PBS before further mixing with C7 (10% w/v in PBS). The volumes of 8-arm-PEG–peptide conjugate solution and C7 were adjusted to achieve a final C:P ratio of 1:1 at a total hydrogel concentration of 10% w/v.

For cell injection studies, the final mixing step with C7 was performed in the barrel of a 28 G insulin syringe. The mixture was allowed to gel for 5 min before injecting into a circular silicone mold (diameter = 4 mm, height = 2 mm) within a 24-well plate at a rate of ~0.5 mL/min (n ≥ 4). For 3D culture studies, the C7 mixing step was performed directly in the silicone mold in a 24-well plate (n ≥ 4), and the mixture was allowed to gel for 5 min before EGM-2MV media addition and incubation in EGM-2MV media. In both studies, cell suspension in PBS was included as control.

To assess cell viability, samples were incubated with D-luciferin (150 μg/mL), and bioluminescence imaging (BLI) was performed with an IVIS imaging system (Xenogen Corp.). The Living Image software (Xenogen Corp.) was used for data acquisition and analysis. BLI intensity was expressed in units of photons/cm^2/s/sr.

Cells were fixed with 4% paraformaldehyde, permeabilized with 0.25% Triton X-100 solution in PBS, and blocked in 5% bovine serum albumin (BSA) and 0.5% Triton X-100 in PBS before incubation in anti-human CD31 primary mouse antibody (1:200, Cell Signaling Technology). All antibodies are dissolved in 2.5% BSA and 0.5% Triton X-100 in PBS. After 3 washes, samples were further incubated with Alexa Fluor 546 F(ab′)2 Fragment of Goat Anti-Mouse IgG (H + L) (1:1000 dilution, Life Technologies), Alexa Fluor 633 Phalloidin (1:300 dilution, Life Technologies), and DAPI (1 μg/mL, Life Technologies) before washing and mounting in ProLong Gold Antifade (Life Technologies). Images of cell morphology were obtained using a Leica TCS SP5 confocal microscope.

2.9. Hindlimb ischemia

Unilateral hindlimb ischemia was induced in male NOD SCID mice (12–16 weeks old) by ligating the left femoral artery, as previously reported [12]. The contralateral limb served as non-ischemic control. Surgery was performed under constant isoflurane anesthesia, and all animal procedures were approved by the Administrative Panel on Laboratory Animal Care at Stanford University. Immediately following ischemia induction, animals were randomly assigned to receive intramuscular (IM) injection in the gastrocnemius muscle (n = 4 in each group), of the following payloads: 1) PBS; 2) MITCH-PEG; 3) hiPSC-ECs and VEGF in PBS; and 4) hiPSC-ECs and VEGF in MITCH-PEG. In this study, MITCH-PEG refers to the 8P2-20k gel variant (10% w/v, C:P ratio = 1:1). Where applicable, 5×10^5 cells and 3 μg of human recombinant $VEGF_{165}$ (R&D systems) were delivered into each mouse.

Animals were euthanized on day 14 and the gastrocnemius tissues were isolated and flash-frozen in O.C.T. compound for cryosectioning and subsequent examination of hematoxylin and eosin (H&E) stained sections by a board-certified veterinary pathologist who was blinded to the goals of the study and the identity of the samples. Histology scores were given to each muscle tissue sample according to the criteria listed in Table 1.

3. Results and discussion

3.1. Design of an avidity-controlled MITCH-PEG system

Inspired by our previously reported Mixing-Induced Two-Component Hydrogel (MITCH) system [1,7,33], these materials (coined MITCH-PEG) also comprise two soluble polymers that assemble into hydrogel networks by specific molecular recognition between WW and proline-rich peptide domains upon simple mixing (Fig. 1). While the

Please cite this article as: W. Mulyasasmita, et al., Avidity-controlled hydrogels for injectable co-delivery of induced pluripotent stem cell-derived endothelial cells and growth fact..., J. Control. Release (2014), http://dx.doi.org/10.1016/j.jconrel.2014.05.015

Table 1
Histology score criteria.

Score	Muscle necrosis	Muscle inflammation (neutrophils and/or macrophages)	Muscle regeneration
0	None	None	None
1	Minimal, scattered	Minimal, scattered	Minimal, scattered
2	Mild, scattered to multifocal	Mild, scattered to multifocal	Mild, scattered to multifocal
3	Moderate, multifocal	Moderate, multifocal	Moderate, multifocal
4	Intense, multifocal to diffuse	Intense, multifocal to diffuse	Intense, multifocal to diffuse

original MITCH system was designed from two, linear, engineered proteins, the MITCH-PEG system described here includes a single, linear, engineered protein (termed C7) and a multi-armed, peptide-modified polyethylene glycol (PEG). The C7 protein contains seven repeats of a computationally derived WW domain [1,34] interspersed with a hydrophilic, random coil peptide sequence [7,35] (Fig. S1). PEG is a highly hydrophilic, FDA-approved polymer that is readily decorated with peptides *via* covalent bioconjugation. To explore the potential tuning of hydrogel properties through avidity effects, an 8-arm PEG was decorated with either a single proline-rich peptide (termed P1) or a double repeat of the proline-rich peptide (P2). We hypothesized that separating the two proline-rich binding peptides within the P2 sequence with a tetraglycine spacer would provide conformational flexibility to avoid steric hindrance upon binding to a single C domain. We further hypothesized that this tetraglycine spacer would be too short to accommodate binding of two C domains simultaneously. Thus, while the P1 and P2 domains both bind to only a single C domain at a given time, the P2 domain should have a higher effective binding strength compared to the P1 domain due to avidity. A Michael-type addition was chosen to bioconjugate the P1 or P2 peptides onto vinyl sulfone-terminated, 8-arm PEG (PEG-VS). This reaction between thiols and vinyl sulfones is a rapid and highly selective reaction that allows the conjugation of cysteine-containing compounds to be performed under aqueous physiological conditions [36,37]. Reaction of cysteine-terminated P1 or P2 peptides with either 20 kDa or 40 kDa 8-arm PEG-VS (Fig. 2a), followed by purification by solvent extraction, generated four variants of 8-arm-PEG–peptide conjugates with high degrees of substitution (73–88% by NMR) (Fig. 2b). Success of the purification was characterized by SDS-PAGE, where only a single molecular weight species was observed for each purified product (Fig. 2c).

3.2. Mechanical properties of MITCH-PEG are a function of component molecular weight and avidity-controlled binding strength

Bulk mechanical properties of hydrogels depend on crosslinking density, which in noncovalent physical hydrogels is dictated by the individual polymer molecular weights, as well as the number and strength of crosslinking binding interactions per polymer unit [38,39]. Star-shaped PEG-VS of various degrees of polymerization and arm numbers are available commercially, providing an off-the-shelf selection of molecular weights and functionality. We used 8-arm-PEG-VS with molecular weights of 20 kDa and 40 kDa as precursors to conjugation. The 4-arm counterparts failed to meet the critical functionality for forming a percolating gel network, as mixing with C7 produced viscous solutions with loss moduli (G'') predominating the storage moduli (G') (data not shown).

To tune the strength of peptide binding without investing in extensive peptide mutagenesis and screening, we take advantage of avidity effects, a multimerization strategy commonly used in antibody engineering to create high-affinity diabodies and triabodies [40]. As confirmation of our avidity peptide design, isothermal titration calorimetry (ITC) revealed that P2 binding with the complementary CC43 WW domain (denoted C1) had an exothermic binding enthalpy two times greater than that of P1-C1 binding (Fig. 3a). The ITC data also confirmed that the tetraglycine linker introduced to confer rotational freedom to the two P domains in P2 was sufficiently short to preclude two C1 domains from binding simultaneously, as no significant changes in binding stoichiometry were detected (Fig. 3a). The increase in C1:P2 binding energy is thus a consequence of prolonged binding duration as a single C1 domain dissociates and re-associates between the two adjacent P domains. In subsequent experimental design and analysis, each pendant peptide group (P1 or P2) in the 8-arm PEG–peptide conjugates was treated as one P unit regardless of multivalency.

Mixing of C7 with permutations of PEG molecular weight (20 kDa or 40 kDa) and binding strength (P1 or P2) creates four hydrogel variants (denoted 8P1-20k, 8P2-20k, 8P1-40k, and 8P2-40k). As expected, decreasing the PEG–peptide molecular weight or increasing the PEG–peptide binding strength resulted in stiffer hydrogels (Fig. 3b). 8P2-20k, with shorter arm length and stronger binding, exhibited the highest storage modulus ($G' = 15.0$ Pa at 10% w/v and a C:P ratio of 1:1). At the same concentration and C:P ratio, 8P1-40k had the lowest storage modulus ($G' = 3.9$ Pa).

Preformed MITCH-PEG hydrogels exhibited thixotropy, or the ability to shear-thin and self-heal. When subjected to linear shearing under alternating low and high shear rates, the materials responded by assuming high and low viscosity values in an instantaneous (<1 s) and

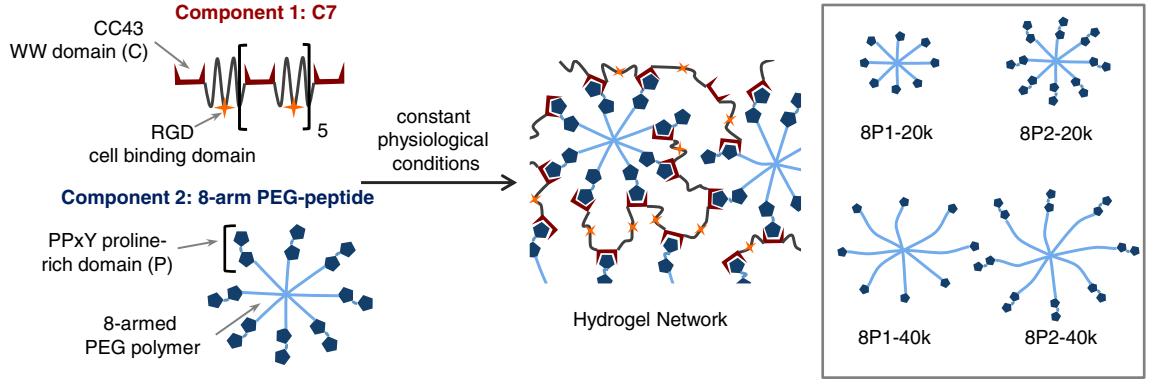

Fig. 1. Schematic of MITCH-PEG hydrogel formation. Component 1 is a recombinant protein copolymer bearing CC43 WW domains (denoted as C) and RGD cell-binding domains. Component 2 is an 8-arm PEG–peptide conjugate bearing complementary proline-rich peptide domains (denoted as P). Simple mixing of the two components results in hydrogel network formation. Inset shows variants of the 8-arm PEG–peptide conjugate, created by varying domain repeat (P1 for one domain or P2 for two domains) and the PEG molecular weight (20 kDa or 40 kDa).

Please cite this article as: W. Mulyasasmita, et al., Avidity-controlled hydrogels for injectable co-delivery of induced pluripotent stem cell-derived endothelial cells and growth fact..., J. Control. Release (2014), http://dx.doi.org/10.1016/j.jconrel.2014.05.015

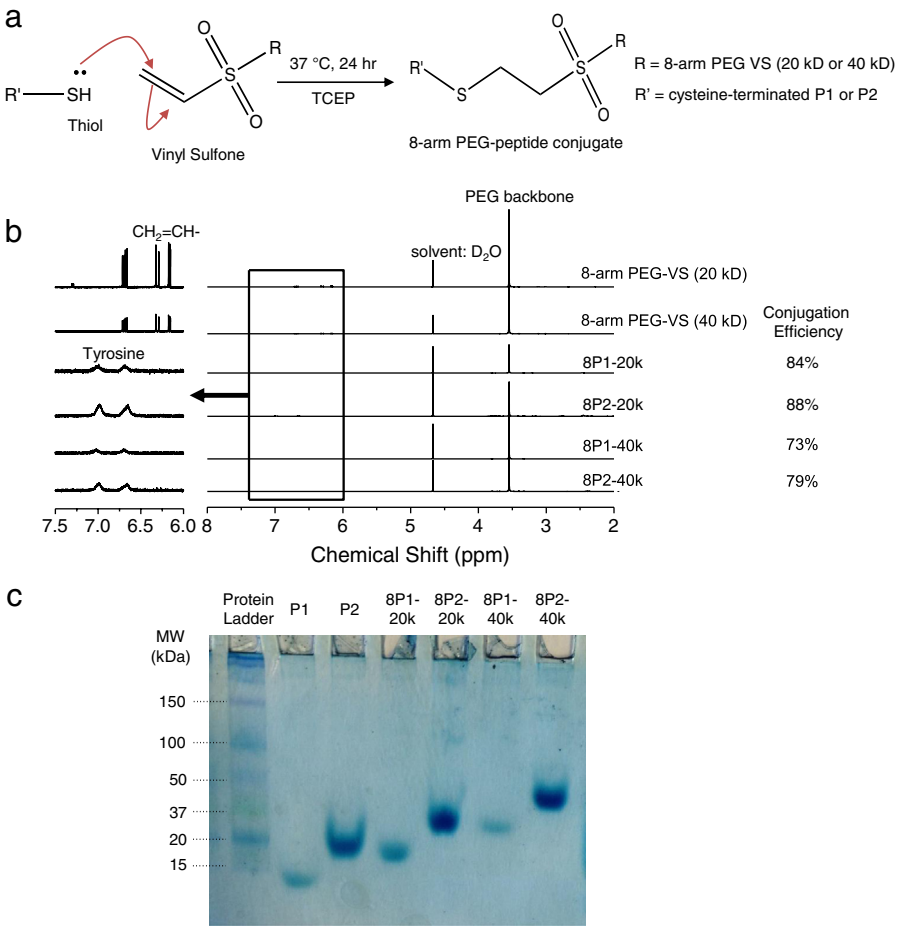

Fig. 2. Characterization of peptide conjugation to PEG. (a) Conjugation reaction scheme by Michael addition. (b) ^{1}H NMR spectra of the 8-arm PEG-VS precursors and the 8-arm PEG–peptide conjugate products. The disappearance of the vinyl (CH_2═CH–) peaks from the precursors and the appearance of tyrosine doublets in the products (inset) confirm the conjugation reaction. Conjugation efficiency was calculated from the tyrosine:PEG backbone peak ratio. (c) Polyacrylamide gel electropherogram of the precursor peptides and the purified 8-arm PEG–peptide conjugates. Only one band is detected for each sample at various molecular weights, indicating purity and success of conjugation. Due to non-denaturing conditions, bands appear at positions different from those expected from the ladder standards.

reversible fashion (Fig. 3c). This sharp yielding transition under high shear is a consequence of transient unbinding between P and C peptides, while reformation of the P–C physical network junctions upon shear removal enables rapid self-healing. MITCH-PEG hydrogels are thus ideal for injectable applications, where the hydrogels must yield and flow as low-viscosity materials under modest hand pressure and then recover the gel state immediately post-injection to prevent cargo sedimentation or diffusion into off-target tissue sites.

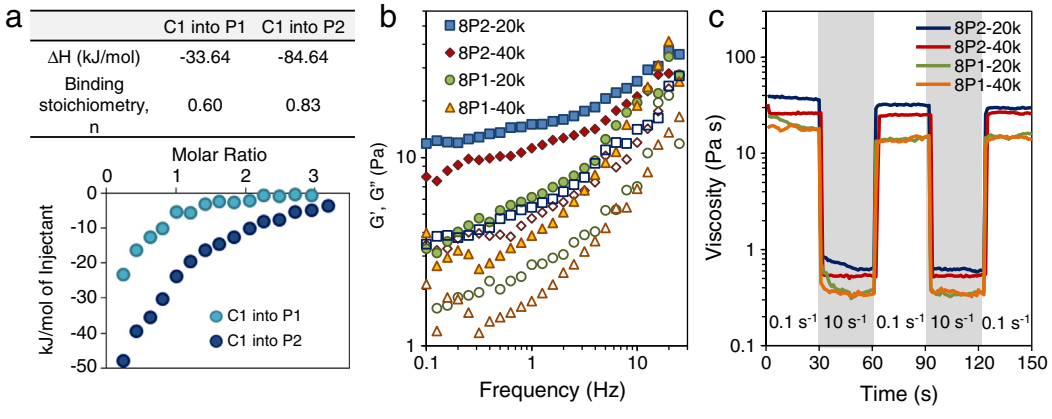

Fig. 3. Dependence of hydrogel shear moduli and thixotropy on crosslinking strength and molecular weight between crosslinks. (a) Binding isotherms obtained from isothermal titration calorimetry (ITC) injections of C1 peptide into P1 or P2. Table shows binding enthalpy and stoichiometry derived from fitting binding isotherms to an independent site model. (b) Storage moduli (G', closed symbols) and loss moduli (G'', open symbols) of MITCH-PEG variants as a function of frequency (10% w/v gels, 5% strain, 37 °C). (c) Linear shear viscosity measured under alternating shear rates, showing shear-thinning and self-healing behavior (10% w/v gels, 30-s durations of 0.1 and 10 s^{-1} shear rate, 37 °C).

Please cite this article as: W. Mulyasasmita, et al., Avidity-controlled hydrogels for injectable co-delivery of induced pluripotent stem cell-derived endothelial cells and growth fact..., J. Control. Release (2014), http://dx.doi.org/10.1016/j.jconrel.2014.05.015

3.3. VEGF delivery from MITCH-PEG with tunable kinetics

MITCH-PEG is an effective vehicle for controlled drug delivery due to several attributes. First, the simple mixing protocol of MITCH-PEG gelation supports growth factor incorporation in its bioactive format without exposing the growth factor to covalent crosslinkers or changes in pH, temperature, or ionic strength. Second, hydrogel mesh size, a key determinant of molecular diffusivity within a network, is easily tunable through appropriate selection of 8-arm-PEG–peptide conjugate.

Crosslinking density dictating hydrogel stiffness is inextricably linked to network mesh size. Therefore, drugs loaded through simple encapsulation in MITCH-PEG diffuse with decreasing mobility in stiffer hydrogel formulations. We used fluorescently-labeled dextran drug analogs and employed a spectroscopic technique called fluorescence recovery after photobleaching (FRAP) [31] as an inexpensive, high throughput method for mapping diffusivity as a function of hydrogel mesh size and cargo molecular weight. A high intensity laser was focused onto a defined volume in the hydrogel where fluorescent dextran had been homogenously encapsulated, resulting in photobleaching. Subsequent diffusion of surrounding unbleached dextran molecules into the photobleached area produced time-dependent fluorescence recovery profiles (Fig. 4a) from which diffusivity constants of the encapsulated dextran molecules were computed (Fig. 4b, c). Diffusivity constants not only decreased with molecular weight, as expected, but also depended on PEG arm length (20 kDa *vs.* 40 kDa) and peptide binding strength (P1 *vs.* P2) in the same order as trends in hydrogel stiffness. Consequently, slowest and fastest diffusion corresponded to diametrically opposite formulations 8P2-20k and 8P1-40k, respectively. Diffusivity constants were also computed for dextran diffusing in growth factor-reduced Matrigel and rat-tail Type I collagen (2.5 mg/mL), two common cell transplantation matrices with comparable storage moduli as MITCH-PEG [33,41]. Diffusivity was significantly slower in MITCH-PEG compared to both Matrigel and Type I collagen (Fig. 4b, c).

While FRAP experiments are material and time efficient, macrodiffusivity determinants such as hydrogel swelling, degradation, and initial burst release from the gel surface are not factored into the analysis. As such, actual bulk release profiles over longer timescales cannot be quantitatively predicted from FRAP data [42]. Release experiments by bulk gel immersion and sampling were therefore performed using the 20 kDa dextran drug analog (Fig. 5a), chosen for its comparable Stokes radius to that of VEGF [43]. Clearly these well controlled *in vitro* studies, which utilize a large excess of static, pristine buffer, do not mimic the microenvironment of an actual *in vivo* transplantation site, where the gel would be confined by the local adjacent tissue and exposed to interstitial fluid flow. Nonetheless, although the absolute values of VEGF release *in vitro* cannot be directly extrapolated to predict *in vivo* release profiles, they can be used to estimate the general trends of release kinetics from different types of matrices [42,44,45].

The kinetics of drug delivery from a hydrogel into a medium is dependent on the loss of matrix material [44], which in physical hydrogels such as MITCH-PEG occurs predominantly by surface erosion rather than internal degradation of matrix polymers. Material was lost steadily after an initial phase of rapid loss, driven in the first few hours of hydrogel submersion by dilution into the medium. Since surface erosion is a function of crosslinking binding strength and density, the overall rates of matrix material loss obeyed the same trend as hydrogel stiffness (Fig. 5b). For example, comparing the effects of avidity, at 72 h significantly less 8P2-20k material has eroded compared to the 8P1-20k material (Fig. 5b). Similarly, comparing the effects of molecular weight, at 72 h significantly less 8P2-20k material has eroded compared to the 8P2-40k material (Fig. 5b). The resulting bulk release curves of dextran were consistent with the underlying trends in hydrogel mechanical properties, mesh size, and erosion rates. For example, comparing the effects of avidity, at 72 h significantly less dextran was released from the 8P2-20k material compared to the 8P1-20k material (Fig. 5a). Similarly, comparing the effects of molecular weight, at 72 h significantly less

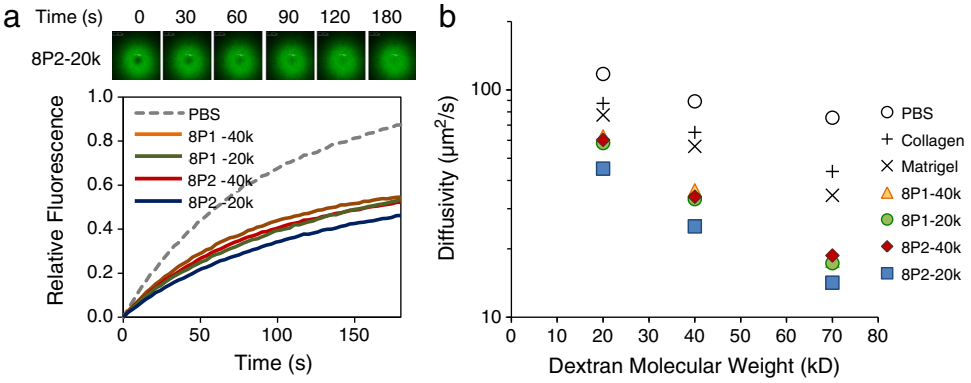

c

	Diffusivity (μm²/s)		
	20 kD dextran	40 kD dextran	70 kD dextran
8P2-20k	45.1 ± 3.8	25.1 ± 2.0	14.2 ± 1.8
8P2-40k	60.3 ± 3.4	33.9 ± 3.4	18.7 ± 3.5
8P1-20k	58.4 ± 5.2	33.1 ± 1.5	17.3 ± 1.9
8P1-40k	62.5 ± 8.1	36.2 ± 2.7	17.7 ± 3.5
Collagen (2.5 mg/ml)	87.3 ± 8.9	65.1 ± 2.8	43.8 ± 4.3
Matrigel	77.6 ± 5.8	56.5 ± 4.8	34.4 ± 2.0
PBS	117.6 ± 6.4	89.1 ± 7.0	75.5 ± 7.8

Fig. 4. FRAP characterization of dextran diffusivity within MITCH-PEG variants. (a) Representative time-lapse fluorescence images of a photobleached area (upper left panel) and the corresponding fluorescence recovery curves obtained from 40 kDa dextran (bottom). (b) Diffusivity constants derived from fluorescence recovery curves are plotted on a semi-logarithmic graph and reported in the table (c). Values obtained from encapsulation in common biomatrices (collagen and Matrigel) and PBS are included for comparison.

Please cite this article as: W. Mulyasasmita, et al., Avidity-controlled hydrogels for injectable co-delivery of induced pluripotent stem cell-derived endothelial cells and growth fact..., J. Control. Release (2014), http://dx.doi.org/10.1016/j.jconrel.2014.05.015

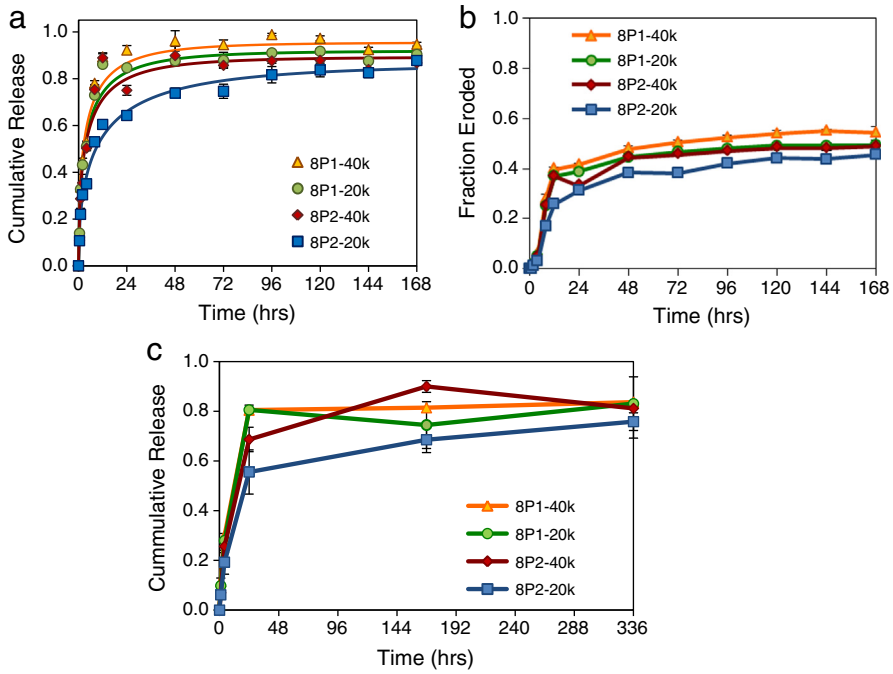

Fig. 5. Kinetics of hydrogel erosion and dextran and VEGF release. (a) Cumulative release curves of 20 kDa dextran from MITCH-PEG into bulk PBS medium. Solid lines represent curve-fits for Fick's 2nd law of diffusion from thin slabs. (b) Cumulative fraction of hydrogel material eroded into bulk PBS medium. (c) Quantification of $VEGF_{165}$ cumulative release by ELISA.

dextran was released from the 8P2-20k material compared to the 8P2-40k material (Fig. 5a). Accordingly, 8P1-40k resulted in the fastest delivery rate (Fig. 5a).

In a previous hindlimb ischemia study, correlational mapping between VEGF concentration and angiogenic sprouting revealed a two-phase profile of high initial availability and low subsequent amounts as the optimal VEGF distribution for normal revascularization [45]. Recombinant human $VEGF_{165}$ released from MITCH-PEG into a medium of PBS was detectable by anti-VEGF monoclonal antibody in sandwich ELISA for up to 14 days (Fig. 5c), indicating the preservation of native tertiary structure. The 8P2-20k hydrogel formulation fulfilled this biphasic release criteria for both VEGF (Fig. 5c) and 20 kDa dextran (Fig. 5a), and was therefore selected as the carrier for subsequent *in vitro* cell culture and *in vivo* hindlimb ischemia experiments.

3.4. MITCH-PEG improves acute post-injection viability of hiPSC-ECs in vitro

During high-shear flow in narrow capillaries or syringe needles, shear zones in thixotropic hydrogels have been observed to localize as narrow bands near the capillary wall while a broad central zone experiences negligible shear [14,15]. Cells transported within the central plug are thus shielded from detrimental mechanical forces, thereby improving cell survival during the injection process. We therefore hypothesized that the thixotropic MITCH-PEG hydrogel would be able to enhance the viability of human induced pluripotent stem cell-derived endothelial cells (hiPSC-ECs) exposed to syringe injection compared to cell delivery in saline alone. To facilitate non-invasive monitoring of cell viability, human induced pluripotent stem cell-derived endothelial cells (hiPSC-ECs) were stably transduced with a double fusion reporter construct encoding firefly-luciferase (Fluc) and enhanced green fluorescent protein (eGFP) under a constitutive ubiquitin promoter, as previously reported [12]. As expected, hiPSC-ECs delivered through a 28 G syringe needle at a flow rate of ~0.5 mL/min experienced a significant loss in cell viability when delivered in saline alone. In contrast, pre-encapsulation of the hiPSC-ECs within the 8P2-20k hydrogels prior to syringe delivery resulted in no loss of cell viability (Fig. 6a).

The recombinant DNA technology used to create the C7 component allows both crosslinking peptides and RGD cell-binding domains to be incorporated into the same protein polymer. As such, beyond structural protection, MITCH-PEG materials are capable of maintaining cell–matrix adhesion through integrin binding, an essential survival signal for endothelial cells (ECs) [46,47]. ECs deprived of integrin signaling rapidly undergo anoikis, a form of programmed cell death commonly experienced by transplanted cells upon matrix detachment [48,49]. Cells encapsulated in 8P2-20k remained proliferative over 4 days of *in vitro* culture (Fig. 6b), implying material cytocompatibility and provision of a pro-survival microenvironment. Visualization of F-actin by confocal microscopy revealed well-spread cytoskeletal stress fiber morphologies, which serve as indirect evidence for integrin binding and focal adhesion formation (Fig. 6b) [50,51]. To evaluate if the various MITCH-PEG formulations could support hiPSC-EC proliferation, the number of viable cells was quantified at day 0 (immediately after injection) and again at day 4. In all four formulations, the number of cells more than doubled during this time, and no statistically significant differences between the four formulations were observed (Fig. 6c).

3.5. Co-delivery of hiPSC-ECs and VEGF in MITCH-PEG improves tissue regeneration and reduces necrosis in the ischemic calf muscle compared to delivery in MITCH-PEG or saline alone

Treatment of murine hindlimb ischemia by hiPSC-EC injection was motivated by the need for a minimally invasive and enduring therapy for PAD [12]. When delivered in liquid medium, hiPSC-ECs were found to induce capillary formation by secreting angiogenic cytokines while directly incorporating into expanding vascular networks [12]. As symptomatic relief generally correlates with the number of viable donor cells [52,53], improving post-transplantation cell survival would solve a major bottleneck in cell regenerative therapy. Treatment of donor cells with pro-survival factors is one strategy for boosting viability [16,17]. VEGF has a range of well-documented pro-survival and pro-proliferation effects on endothelial cells [54]. In the current study, luciferase-positive hiPSC-ECs were co-injected with VEGF intramuscularly into the ischemic calf of non-obese diabetic severe combined immune deficient (NOD SCID) mice immediately following femoral

Please cite this article as: W. Mulyasasmita, et al., Avidity-controlled hydrogels for injectable co-delivery of induced pluripotent stem cell-derived endothelial cells and growth fact..., J. Control. Release (2014), http://dx.doi.org/10.1016/j.jconrel.2014.05.015

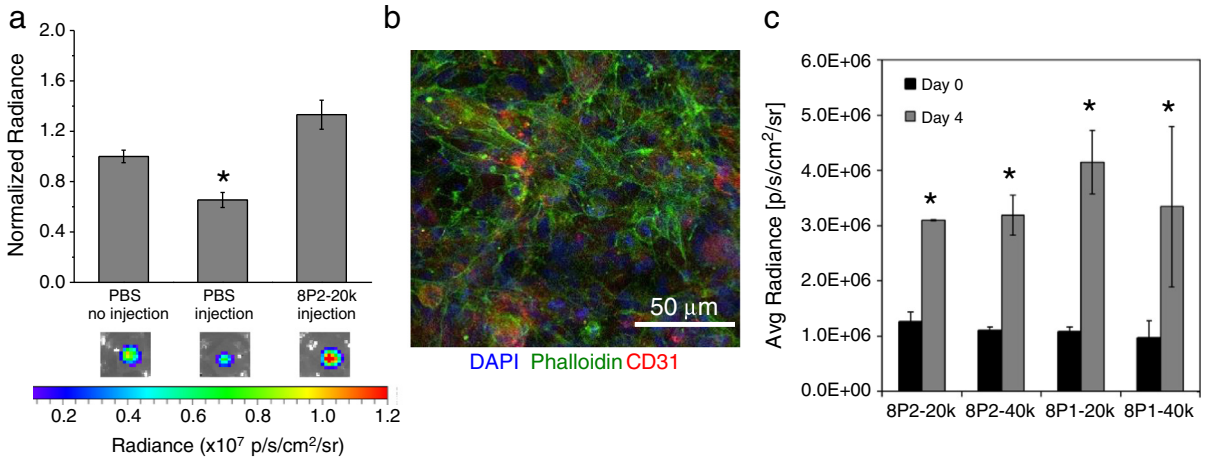

Fig. 6. (a) Bioluminescence imaging (BLI) quantification of acute hiPSC-EC viability following *in vitro* injection. Pre-encapsulation of hiPSC-ECs (Fluc+) in MITCHs improved post-injection viability relative to injected cells suspended in PBS, $^*p < 0.05$. (b) Three-dimensional (3D) culture of hiPSC-ECs in 8P2-20k variant of MITCH-PEG. Visualization of cell morphology at day 4 of encapsulation by confocal immunofluorescence. Cell nuclei shown by DAPI staining in blue, F-actin cytoskeleton by phalloidin staining in green, and CD31 endothelial cell marker in red. (c) BLI quantification of hiPSC-ECs within four different variants of MITCH-PEG at days 0 and 4 post-injection, $^*p < 0.05$. (For interpretation of the references to color in this figure legend, the reader is referred to the web version of this article.)

artery ligation either using 8P2-20k as a delivery vehicle or delivery in phosphate-buffered saline (PBS). The two goals of the study were to determine (i) if the injection of MITCH-PEG alone would have any beneficial or adverse effects and (ii) if MITCH-PEG could be used to co-deliver functional hiPSC-ECs and VEGF.

Superficially, the affected hindpaw digits of all mice receiving hiPSC-ECs and VEGF co-delivered within MITCH-PEG developed sporadic necrosis of the nails only, with no necrosis of the digits observed. In contrast, the 75% of mice receiving hiPSC-ECs and VEGF co-delivered within PBS were observed to have partial or full digit necrosis with subsequent self-amputation. To evaluate the extent of inflammation, necrosis, and regeneration, skeletal muscle tissues were isolated and cryosectioned for histologic evaluation two weeks post-injection. Sections from non-injured muscle tissue served as a control. Histology scores indicated that no statistically significant differences in inflammation occurred across all sample groups (Fig. 7a), suggesting that all injected samples were well tolerated. Interestingly, injection of 8P2-20k alone into the ischemic site (without encapsulated hiPSC-ECs or VEGF) resulted in statistically higher levels of both necrosis and regeneration compared to delivery of PBS alone (Fig. 7b, c). The co-delivery of hiPSC-ECs and VEGF, within either 8P2-20k or PBS, significantly reduced necrosis and was statistically similar to uninjured controls (Fig. 7b). The regeneration scores demonstrate that hiPSC-EC/VEGF co-delivery, within either 8P2-20k or PBS, induced the development of a viable, robust regenerative response by the myofibers (Fig. 7c). These effects were statistically different from the uninjured control (where no regeneration is expected) and from the delivery of 8P2-20k or PBS alone. Taken together, these data confirm that the 8P2-20k gel can be used as a carrier to co-deliver hiPSC-ECs and VEGF to induce regeneration and decrease necrosis. However, in contrast to the superficial scoring of nail/digit necrosis, the histological analysis did not demonstrate any significant benefits to co-delivery using the 8P2-20k gel compared to delivery in PBS.

Representative histological slices confirm the pathologist scoring. In the control mice (no ischemic injury), the skeletal muscle is histologically normal, characterized by myofibers with a roughly angular shape and delineated cell membranes enclosing homogenous, eosinophilic (red) sarcoplasm; sarcoplasm with few or no clear spaces (*i.e.* glycogen accumulation); nuclei that are flattened and dark with eccentric location at the periphery of the myofiber; and a minimal amount of connective tissues between myofibers, resulting in close packing of the myofibers (Fig. 7d). In the ischemic mice with PBS delivery, there are changes consistent with inflammation and myofiber necrosis (Fig. 7e). The inflammation is characterized by expansion of the connective tissues between myofibers (black asterisk) due to poorly staining edema fluid and loose, disorganized collagen deposition (*i.e.* early fibrosis). The expanded connective tissue also contains some neutrophils and macrophages (*i.e.* nucleated inflammatory cells). The myofiber necrosis is characterized by swelling of myofibers with increased cell diameter and loss of angular shape, hypereosinophilia (deeper red) of the sarcoplasm, a "moth-eaten" fragmentation appearance of the sarcoplasm, presence of centralized clear spaces in the sarcoplasm (*i.e.* glycogen accumulation, which is indicative of cellular stress and injury), loss of cell membrane integrity, and loss of nuclei. In the ischemic mice receiving the 8P2-20k MITCH-PEG injections, the changes are similar to those receiving PBS injection except that some myofibers have survived the ischemia (lower right corner) and show an early regenerative response (Fig. 7f). The surviving myofibers are much smaller and contain smaller amounts of glycogen (*i.e.* small clear spaces) compared with the necrotic myofibers. The nuclei are more round and plump and located centrally, both indicative of a regenerative response.

In the ischemic mice that received co-delivery of hiPSC-ECs and VEGF using a PBS carrier, there are milder inflammatory changes, a robust but still early myofiber regenerative response, and no evidence for necrosis (Fig. 7g). The inflammation is composed of much less edema, small scattered amounts of collagen deposition, and few inflammatory cells in the connective tissues (white asterisk) compared to the mice injected with the PBS carrier or the MITCH-PEG carrier alone. The myofiber regeneration appears more robust than in the mice receiving only the MITCH-PEG carrier, with the myofibers appearing larger; however, the response is still early — myofiber shape and size is quite variable, there is substantial glycogen accumulation inside the sarcoplasm, and the nuclei remain centralized and plump in shape. Finally, in the ischemic mice that received co-delivery of hiPSC-ECs and VEGF using the MITCH-PEG carrier, there is only minimal inflammation present and there is no necrosis evident (Fig. 7h). The inflammation comprises of minimal amounts of fibrosis with minimal edema and occasional inflammatory cells in the connective tissues. The myofibers all appear in a more mature stage of regeneration, the features of which include more uniform myofiber shape and size, the presence of smaller amounts of glycogen in the sarcoplasm, and multiple central nuclei that are more

Please cite this article as: W. Mulyasasmita, et al., Avidity-controlled hydrogels for injectable co-delivery of induced pluripotent stem cell-derived endothelial cells and growth fact..., J. Control. Release (2014), http://dx.doi.org/10.1016/j.jconrel.2014.05.015

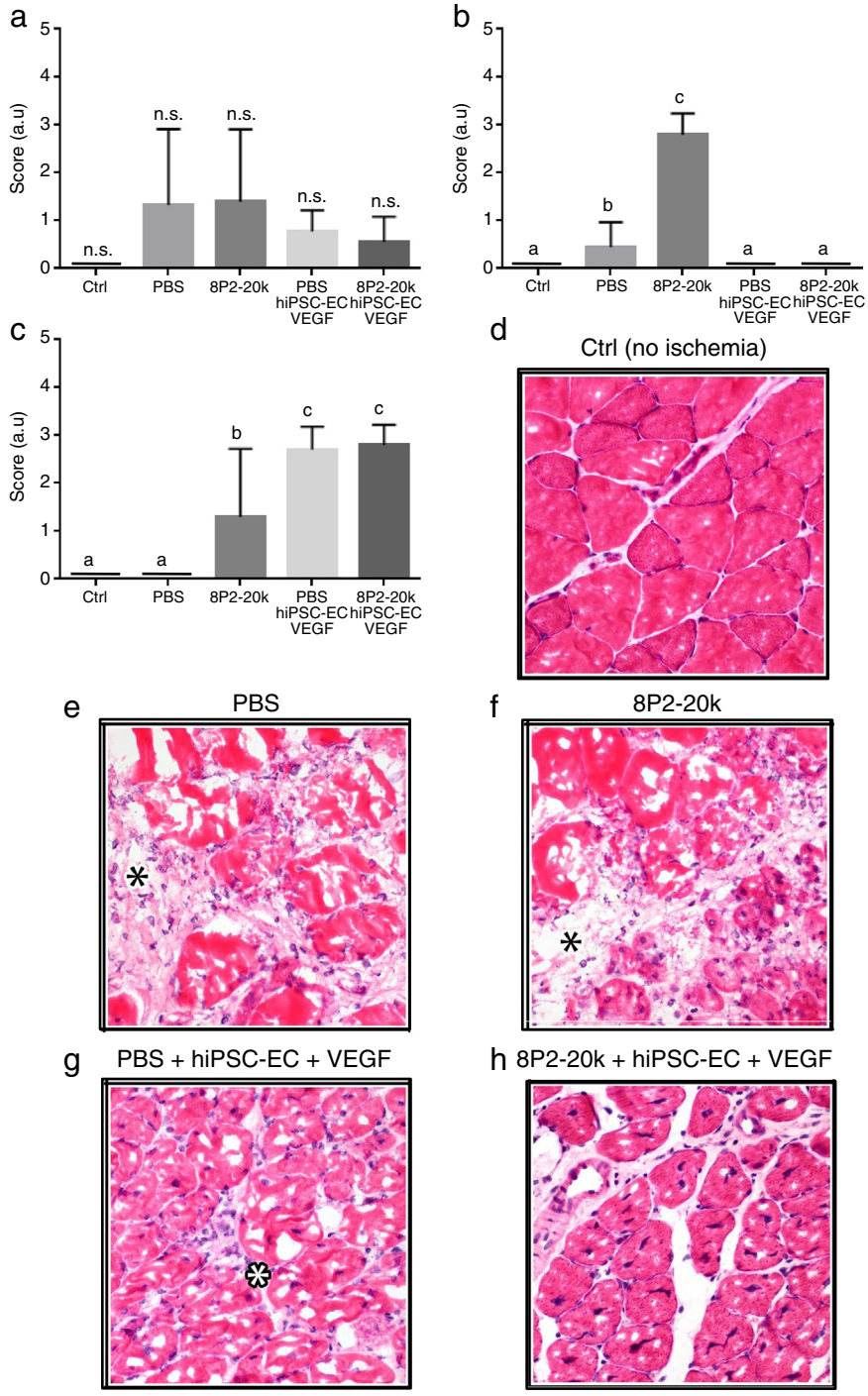

Fig. 7. Histology scores of (a) inflammation, (b) necrosis, and (c) regeneration for a mouse hindlimb ischemia injury model. Scores were evaluated according to the criteria listed in Table 1. Different lowercase letters denote statistically different outcomes, as assessed by ANOVA with Tukey post-hoc test, $p < 0.05$, (n.s. = not significant). (d–h) Photomicrographs of cryosectioned samples of skeletal muscles 14 days after femoral artery ligation-induced ischemia. Hematoxylin and eosin (H&E) stained images of muscle tissue explants for (d) control tissue with no ischemia and ischemic tissue injected with (e) PBS, (f) 8P2-20k, (g) hiPSC-ECs and VEGF in PBS, and (h) hiPSC-ECs and VEGF in 8P2-20k. Inflammation, characterized by expansion of the connective tissues between myofibers, is marked with a black asterisk in panels (e) and (f). Inflammatory cells in the connective tissues are marked with a white asterisk in panel (g).

condensed and flattened. Taken together, these data suggest that functional co-delivery of hiPSC-ECs and VEGF can be achieved using a novel, injectable MITCH-PEG carrier.

4. Conclusions

Here we present a biomimetic strategy to control hydrogel mechanical properties and drug release kinetics by designing avidity peptides that control the hydrogel physical crosslinking. The avidity peptides, which presented two binding domains in close proximity, more than doubled the effective enthalpy of binding compared to a single domain alone. These avidity peptides were bioconjugated to a multi-armed PEG molecule to enable spontaneous hetero-assembly with a linear, engineered protein through physical, molecular recognition of the peptide structure. This Mixing-Induced Two-Component Hydrogel (MITCH) strategy is able to encapsulate viable hiPSC-ECs and

bioactive VEGF without the use of chemical crosslinkers or any changes in temperature, pH, or ionic concentration. The crosslinking density in these MITCH-PEG materials was tuned both by altering the PEG molecular weight and by exploiting peptide avidity. As expected, increases in crosslinking density resulted in stiffer hydrogels with slower diffusion, surface erosion, and bulk release kinetics. These materials may be well suited for regenerative medicine applications that involve direct injection of stem cell-derived therapies. As a proof of principle, hiPSC-ECs remained proliferative when encapsulated and cultured within MITCH-PEG. Furthermore, pre-encapsulation of hiPSC-ECs within MITCH-PEG was found to sustain cell viability when subjected to injection through a 28 G syringe needle. In a hindlimb ischemia injury model, co-delivery of hiPSC-ECs with VEGF from MITCH-PEG reduced necrosis while improved muscle regeneration compared to delivery of saline or MITCH-PEG alone. Taken together, these data suggest that these injectable materials address several challenges in stem cell-based therapeutics by providing a matrix that protects cells from damage during syringe needle injection, that presents an integrin ligand to promote cell adhesion and to prevent anoikis, and that enables the co-delivery and sustained release of bioactive pro-survival factors. These results warrant future preclinical studies into the biocompatibility and biodistribution of MITCH-PEG and its degradation products in models of ischemic injury and disease.

Acknowledgment

We acknowledge support from the Stanford Graduate Fellows Program and Siebel Scholars Program (W.M.), National Science Foundation (DMR-0846363 to S.H.), NIH (R01-DK085720 and DP2-OD006477 to S.H. and R00-HL098688 to N.H.), Genentech (1-PTD), and CIRM (RT2-01938). The authors thank Karen Dubbin for FRAP method optimization, and Tim Doyle (Stanford Molecular Imaging Program) for assistance with BLI.

Appendix A. Supplementary data

Supplementary data showing the full amino acid sequences of all engineered proteins and peptides reported in this article can be found online at http://dx.doi.org/10.1016/j.jconrel.2014.05.015.

References

[1] C.T. Wong Po Foo, J.S. Lee, W. Mulyasasmita, A. Parisi-Amon, S.C. Heilshorn, Two-component protein-engineered physical hydrogels for cell encapsulation, Proc. Natl. Acad. Sci. U. S. A. 106 (2009) 22067–22072.
[2] H.D. Lu, M.B. Charati, I.L. Kim, J.A. Burdick, Injectable shear-thinning hydrogels engineered with a self-assembling Dock-and-Lock mechanism, Biomaterials 33 (2012) 2145–2153.
[3] H.D. Lu, D.E. Soranno, C.B. Rodell, I.L. Kim, J.A. Burdick, Secondary photocrosslinking of injectable shear-thinning dock-and-lock hydrogels, Adv. Healthc. Mater. 2 (2013) 1028–1036.
[4] F. Ito, K. Usui, D. Kawahara, A. Suenaga, T. Maki, S. Kidoaki, H. Suzuki, M. Taiji, M. Itoh, Y. Hayashizaki, T. Matsuda, Reversible hydrogel formation driven by protein–peptide-specific interaction and chondrocyte entrapment, Biomaterials 31 (2010) 58–66.
[5] T.Z. Grove, C.O. Osuji, J.D. Forster, E.R. Dufresne, L. Regan, Stimuli-responsive smart gels realized via modular protein design, J. Am. Chem. Soc. 132 (2010) 14024–14026.
[6] J. Wang, J. Zhang, X. Zhang, H. Zhou, A protein-based hydrogel for in vitro expansion of mesenchymal stem cells, PLoS One 8 (2013) e75727.
[7] W. Mulyasasmita, J.S. Lee, S.C. Heilshorn, Molecular-level engineering of protein physical hydrogels for predictive sol–gel phase behavior, Biomacromolecules 12 (2011) 3406–3411.
[8] S. Hong, P.R. Leroueil, I.J. Majoros, B.G. Orr, J.R. Baker Jr., M.M. Banaszak Holl, The binding avidity of a nanoparticle-based multivalent targeted drug delivery platform, Chem. Biol. 14 (2007) 107–115.
[9] A. Barnard, D.K. Smith, Self-assembled multivalency: dynamic ligand arrays for high-affinity binding, Angew. Chem. Int. Ed. Engl. 51 (2012) 6572–6581.
[10] D. Grunstein, M. Maglinao, R. Kikkeri, M. Collot, K. Barylyuk, B. Lepenies, F. Kamena, R. Zenobi, P.H. Seeberger, Hexameric supramolecular scaffold orients carbohydrates to sense bacteria, J. Am. Chem. Soc. 133 (2011) 13957–13966.
[11] N.F. Huang, J. Okogbaa, A. Babakhanyan, J.P. Cooke, Bioluminescence imaging of stem cell-based therapeutics for vascular regeneration, Theranostics 2 (2012) 346–354.
[12] A.J. Rufaihah, N.F. Huang, S. Jame, J.C. Lee, H.N. Nguyen, B. Byers, A. De, J. Okogbaa, M. Rollins, R. Reijo-Pera, S.S. Gambhir, J.P. Cooke, Endothelial cells derived from human iPSCS increase capillary density and improve perfusion in a mouse model of peripheral arterial disease, Arterioscler. Thromb. Vasc. Biol. 31 (2011) e72–79.
[13] B.A. Aguado, W. Mulyasasmita, J. Su, K.J. Lampe, S.C. Heilshorn, Improving viability of stem cells during syringe needle flow through the design of hydrogel cell carriers, Tissue Eng. A 18 (2012) 806–815.
[14] C. Yan, M.E. Mackay, K. Czymmek, R.P. Nagarkar, J.P. Schneider, D.J. Pochan, Injectable solid peptide hydrogel as a cell carrier: effects of shear flow on hydrogels and cell payload, Langmuir 28 (2012) 6076–6087.
[15] B.D. Olsen, J.A. Kornfield, D.A. Tirrell, Yielding behavior in injectable hydrogels from telechelic proteins, Macromolecules 43 (2010) 9094–9099.
[16] M.A. Laflamme, K.Y. Chen, A.V. Naumova, V. Muskheli, J.A. Fugate, S.K. Dupras, H. Reinecke, C. Xu, M. Hassanipour, S. Police, C. O'Sullivan, L. Collins, Y. Chen, E. Minami, E.A. Gill, S. Ueno, C. Yuan, J. Gold, C.E. Murry, Cardiomyocytes derived from human embryonic stem cells in pro-survival factors enhance function of infarcted rat hearts, Nat. Biotechnol. 25 (2007) 1015–1024.
[17] H. Haider, M. Ashraf, Strategies to promote donor cell survival: combining preconditioning approach with stem cell transplantation, J. Mol. Cell. Cardiol. 45 (2008) 554–566.
[18] S.M. Ryan, G. Mantovani, X. Wang, D.M. Haddleton, D.J. Brayden, Advances in PEGylation of important biotech molecules: delivery aspects, Expert Opin. Drug Deliv. 5 (2008) 371–383.
[19] H. Sugimoto, Y. Hamano, D. Charytan, D. Cosgrove, M. Kieran, A. Sudhakar, R. Kalluri, Neutralization of circulating vascular endothelial growth factor (VEGF) by anti-VEGF antibodies and soluble VEGF receptor 1 (sFlt-1) induces proteinuria, J. Biol. Chem. 278 (2003) 12605–12608.
[20] G. von Degenfeld, A. Banfi, M.L. Springer, R.A. Wagner, J. Jacobi, C.R. Ozawa, M.J. Merchant, J.P. Cooke, H.M. Blau, Microenvironmental VEGF distribution is critical for stable and functional vessel growth in ischemia, FASEB J. 20 (2006) 2657–2659.
[21] J. Tongers, J.G. Roncalli, D.W. Losordo, Therapeutic angiogenesis for critical limb ischemia — microvascular therapies coming of age, Circulation 118 (2008) 9–16.
[22] G.P. Fadini, C. Agostini, A. Avogaro, Autologous stem cell therapy for peripheral arterial disease. Meta-analysis and systematic review of the literature, Atherosclerosis 209 (2010) 10–17.
[23] T.P. Richardson, M.C. Peters, A.B. Ennett, D.J. Mooney, Polymeric system for dual growth factor delivery, Nat. Biotechnol. 19 (2001) 1029–1034.
[24] S.M. Jay, B.R. Shepherd, J.P. Bertram, J.S. Pober, W.M. Saltzman, Engineering of multifunctional gels integrating highly efficient growth factor delivery with endothelial cell transplantation, FASEB J. 22 (2008) 2949–2956.
[25] H.J. Kong, E.S. Kim, Y.-C. Huang, D.J. Mooney, Design of biodegradable hydrogel for the local and sustained delivery of angiogenic plasmid DNA, Pharm. Res. 25 (2008) 1230–1238.
[26] H. Layman, A.A. Rahnemai-Azar, S.M. Pham, G. Tsechpenakis, F.M. Andreopoulos, Synergistic angiogenic effect of codelivering fibroblast growth factor 2 and granulocyte-colony stimulating factor from fibrin scaffolds and bone marrow transplantation in critical limb ischemia, Tissue Eng. A 17 (2011) 243–254.
[27] K. Doi, T. Ikeda, A. Marui, T. Kushibiki, Y. Arai, K. Hirose, Y. Soga, A. Iwakura, K. Ueyama, K. Yamahara, H. Itoh, K. Nishimura, Y. Tabata, M. Komeda, Enhanced angiogenesis by gelatin hydrogels incorporating basic fibroblast growth factor in rabbit model of hind limb ischemia, Heart Vessel. 22 (2007) 104–108.
[28] J. Lee, S.H. Bhang, H. Park, B.-S. Kim, K.Y. Lee, Active blood vessel formation in the ischemic hindlimb mouse model using a microsphere/hydrogel combination system, Pharm. Res. 27 (2010) 767–774.
[29] E. Ruvinov, J. Leor, S. Cohen, The effects of controlled HGF delivery from an affinity-binding alginate biomaterial on angiogenesis and blood perfusion in a hindlimb ischemia model, Biomaterials 31 (2010) 4573–4582.
[30] M.J. Webber, J. Tongers, C.J. Newcomb, K.-T. Marquardt, J. Bauersachs, D.W. Losordo, S.I. Stupp, Supramolecular nanostructures that mimic VEGF as a strategy for ischemic tissue repair, Proc. Natl. Acad. Sci. U. S. A. 108 (2011) 13438–13443.
[31] P. Jonsson, M.P. Jonsson, J.O. Tegenfeldt, F. Hook, A method improving the accuracy of fluorescence recovery after photobleaching analysis, Biophys. J. 95 (2008) 5334–5348.
[32] A.J. Rufaihah, N.F. Huang, J. Kim, J. Herold, K.S. Volz, T.S. Park, J.C. Lee, E.T. Zambidis, R. Reijo-Pera, J.P. Cooke, Human induced pluripotent stem cell-derived endothelial cells exhibit functional heterogeneity, Am. J. Transl. Res. 5 (2013) 21–35.
[33] A. Parisi-Amon, W. Mulyasasmita, C. Chung, S.C. Heilshorn, Protein-engineered injectable hydrogel to improve retention of transplanted adipose-derived stem cells, Adv. Healthc. Mater. 2 (2013) 428–432.
[34] W.P. Russ, D.M. Lowery, P. Mishra, M.B. Yaffe, R. Ranganathan, Natural-like function in artificial WW domains, Nature 437 (2005) 579–583.
[35] W.A. Petka, J.L. Harden, K.P. McGrath, D. Wirtz, D.A. Tirrell, Reversible hydrogels from self-assembling artificial proteins, Science 281 (1998) 389–392.
[36] M.P. Lutolf, J.A. Hubbell, Synthesis and physicochemical characterization of end-linked poly(ethylene glycol)-co-peptide hydrogels formed by Michael-type addition, Biomacromolecules 4 (2003) 713–722.
[37] M.P. Lutolf, G.P. Raeber, A.H. Zisch, N. Tirelli, J.A. Hubbell, Cell-responsive synthetic hydrogels, Adv. Mater. 15 (2003) 888–892.
[38] P.J. Flory, Molecular size distributions in three dimensional polymers. I. Gelation, J. Am. Chem. Soc. 63 (1941) 3083–3090.
[39] W.H. Stockmayer, Theory of molecular size distribution and gel formation in branched-chain polymers, J. Chem. Phys. 11 (1943) 45–55.
[40] A. Todorovska, R.C. Roovers, O. Dolezal, A.A. Kortt, H.R. Hoogenboom, P.J. Hudson, Design and application of diabodies, triabodies and tetrabodies for cancer targeting, J. Immunol. Methods 248 (2001) 47–66.

[41] M.H. Zaman, L.M. Trapani, A.L. Sieminski, D. Mackellar, H. Gong, R.D. Kamm, A. Wells, D.A. Lauffenburger, P. Matsudaira, Migration of tumor cells in 3D matrices is governed by matrix stiffness along with cell-matrix adhesion and proteolysis, Proc. Natl. Acad. Sci. U. S. A. 103 (2006) 10889–10894.
[42] F. Brandl, F. Kastner, R.M. Gschwind, T. Blunk, J. Tessmar, A. Gopferich, Hydrogel-based drug delivery systems: comparison of drug diffusivity and release kinetics, J. Control. Release 142 (2010) 221–228.
[43] V. Eremina, J.A. Jefferson, J. Kowalewska, H. Hochster, M. Haas, J. Weisstuch, C. Richardson, J.B. Kopp, M.G. Kabir, P.H. Backx, H.P. Gerber, N. Ferrara, L. Barisoni, C. E. Alpers, S.E. Quaggin, VEGF inhibition and renal thrombotic microangiopathy, N. Engl. J. Med. 358 (2008) 1129–1136.
[44] Y. Fu, W.J. Kao, Drug release kinetics and transport mechanisms of non-degradable and degradable polymeric delivery systems, Expert Opin. Drug Deliv. 7 (2010) 429–444.
[45] E.A. Silva, D.J. Mooney, Effects of VEGF temporal and spatial presentation on angiogenesis, Biomaterials 31 (2010) 1235–1241.
[46] S. Stromblad, D.A. Cheresh, Integrins, angiogenesis and vascular cell survival, Chem. Biol. 3 (1996) 881–885.
[47] F. Re, A. Zanetti, M. Sironi, N. Polentarutti, L. Lanfrancone, E. Dejana, F. Colotta, Inhibition of anchorage-dependent cell spreading triggers apoptosis in cultured human endothelial cells, J. Cell Biol. 127 (1994) 537–546.
[48] E. Chavakis, S. Dimmeler, Regulation of endothelial cell survival and apoptosis during angiogenesis, Arterioscler. Thromb. Vasc. Biol. 22 (2002) 887–893.
[49] J.B. Michel, Anoikis in the cardiovascular system: known and unknown extracellular mediators, Arterioscler. Thromb. Vasc. Biol. 23 (2003) 2146–2154.
[50] F.G. Giancotti, E. Ruoslahti, Integrin signaling, Science 285 (1999) 1028–1032.
[51] S.I. Fraley, Y. Feng, R. Krishnamurthy, D.H. Kim, A. Celedon, G.D. Longmore, D. Wirtz, A distinctive role for focal adhesion proteins in three-dimensional cell motility, Nat. Cell Biol. 12 (2010) 598–604.
[52] A. Le Huu, A. Paul, L. Xu, S. Prakash, D. Shum-Tim, Recent advancements in tissue engineering for stem cell-based cardiac therapies, Ther. Deliv. 4 (2013) 503–516.
[53] Z. Raval, D.W. Losordo, Cell therapy of peripheral arterial disease: from experimental findings to clinical trials, Circ. Res. 112 (2013) 1288–1302.
[54] N. Ferrara, H.P. Gerber, J. LeCouter, The biology of VEGF and its receptors, Nat. Med. 9 (2003) 669–676

Please cite this article as: W. Mulyasasmita, et al., Avidity-controlled hydrogels for injectable co-delivery of induced pluripotent stem cell-derived endothelial cells and growth fact..., J. Control. Release (2014), http://dx.doi.org/10.1016/j.jconrel.2014.05.015